Title

CONFIRMATION OF THE MISSING-ROW MODEL WITH THREE-LAYER RELAXATIONS FOR THE RECONSTRUCTED Ir (110)-(1x2) SURFACE

Authors

Chan, C.-M.
Hove, M.A. Van

Publication Date

1985-08-01

UC-25
LBL-18667 Revised
Preprint

Lawrence Berkeley Laboratory
UNIVERSITY OF CALIFORNIA

Materials & Molecular Research Division

Submitted to Surface Science

CONFIRMATION OF THE MISSING-ROW MODEL WITH THREE-LAYER RELAXATIONS FOR THE RECONSTRUCTED Ir(110)-(1x2) SURFACE

C.-M. Chan and M.A. Van Hove

August 1985

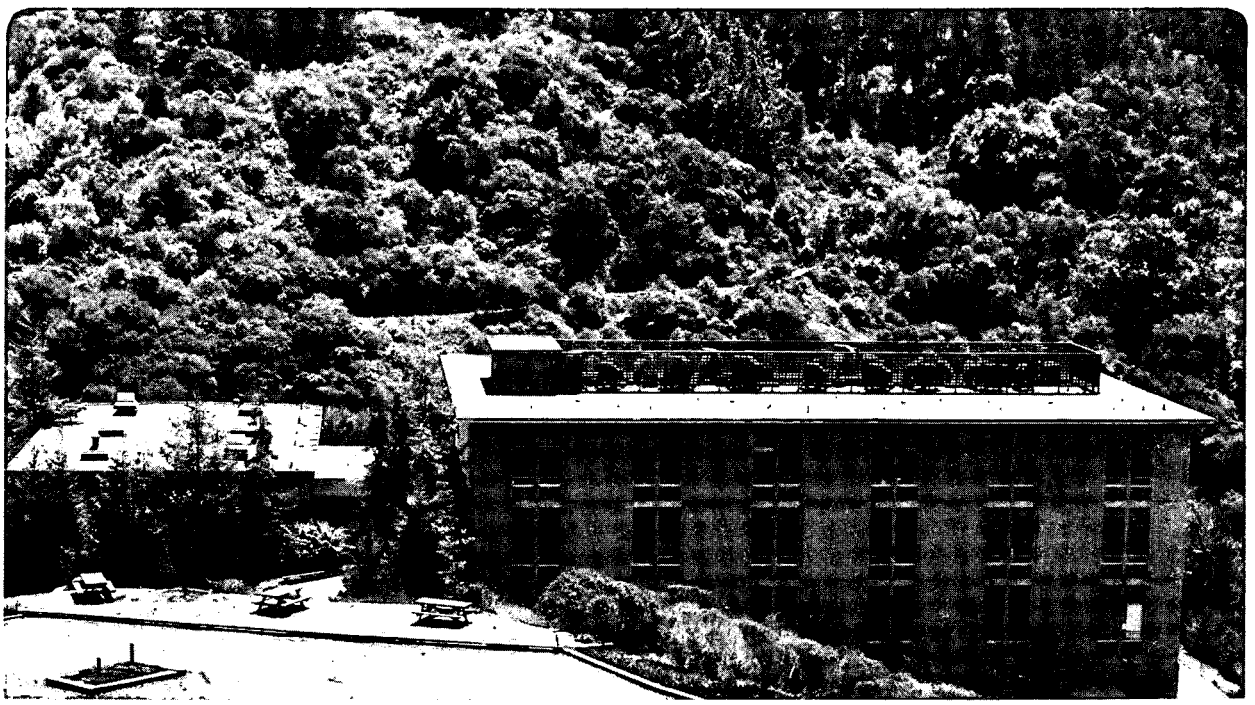

Prepared for the U.S. Department of Energy under Contract DE-AC03-76SF00098

DISCLAIMER

LBL-18667/Revised

Confirmation of the Missing-Row Model With Three-Layer Relaxations for the Reconstructed Ir(110)-(1x2) Surface

by

C.-M. Chan
Corporate Technology
Raychem Corporation
300 Constitution Drive
Menlo Park, CA 94025

and

M. A. Van Hove
Materials and Molecular Research Division
Lawrence Berkeley Laboratory
and
Department of Chemistry
University of California
Berkeley, CA 94720

Submitted to Surface Science
August, 1985

Abstract

The reconstruction of Ir(110)-(1x2) has been re-analyzed by low-energy electron diffraction. In this study, the missing-row model with paired rows in the second layer and buckled rows in the third layer, as well as the Bonzel-Ferrer (sawtooth) model have been examined. In addition, two other models, which are obtained by putting the missing-row atoms back onto the surface in other sites, have also been considered. It is found that the missing-row model with paired rows in the second layer and buckled rows in the third layer gives the best R-factor among all the models considered in this study. This missing-row model with a three-layer reconstruction is thus proposed to solve the Ir(110)-(1x2) structure.

1. Introduction

Much work has been performed on the structure of the (1x2) reconstructions of the clean Ir, Pt and Au(110) surfaces, which are believed to be mutually similar. Several models have been discussed, foremost of which is the missing-row model, cf. Figures 1 and 2. Also prominent is the "sawtooth" model of Bonzel and Ferrer (1), cf. Figure 3. Early LEED work on Ir(110) (2, 3) clearly favored the missing-row model over several other models, but did not consider the sawtooth model, which was proposed later. LEED analyses of the (1x2) reconstructions of Pt(110) (4, 5) and Au(110) (6, 7) were, until recently, inconclusive; some of these analyses included the sawtooth model (5, 7). The missing-row model has been clearly favored by the results derived from a number of other techniques; namely, for Ir(110), Field Ion Microscopy (8), and for Au(110), X-ray diffraction (9), Scanning Tunneling Microscopy (10), High-Resolution Electron Microscopy (11) and High-Energy Ion Scattering (12). Atom diffraction done on Pt(110) could not easily distinguish between the missing-row and the sawtooth models, but could rule out many other models (13, 15). Total-energy calculations did strongly favor the missing-row model over the sawtooth model for Ir(110) (16), Pt(110) (16) and Au(110) (16, 17). A recent re-analysis of the Au(110)-(1x2) LEED data, allowing deeper relaxations than before (namely, a three-layer relaxation) has also convincingly favored the missing-row model (18).

The theory-experiment agreement in the previous LEED study (2, 3) for Ir(110)-(1x2) was far superior to the case of the earlier analyses of

Pt(110) (4, 5) and Au(110) (6, 7), and comparable to the recent LEED study of Au(110) (18). Also, good theory-experiment agreement was obtained in LEED (19) for Ir(110)-c(2x2)O. Therefore, the Ir(110) surface presents a very favorable case for investigating the reconstruction by LEED. Since our previous work (2, 3) did not consider the sawtooth model or large relaxations or multi-layer relaxations within the missing-row model, we here extend the LEED study for Ir(110) to these structures. Large expansions are suggested by results on Au(110) obtained by several non-LEED techniques (9, 11, 12). At the same time, we have now considered a few alternate models inspired by the sawtooth model: the "hollow-on-facet" and "ridge" models, defined in Section 3. Just like the sawtooth model, these two new models require only small atomic motions to switch between an ideal (1x1) structure and the (1x2) reconstruction.

2. Experimental Procedure

The experimental procedure was described in detail elsewhere (2, 3); only a brief description will be given here. The experiments were performed in a UHV chamber which had a base pressure of approximately 5×10^{-11} torr. The Ir single crystal was cleaned by Ar^+ bombardment and a series of treatments in 5×10^{-8} torr of oxygen at 800K. The clean surface, after annealing at 1600K in vacuum, exhibited the (1x2) superstructure.

Twenty LEED intensity-voltage (I-V) spectra consisting of ten half-order beams and ten integral-order beams were collected with a rotatable Faraday cup at approximately 2eV intervals. To confirm that the data were reproducible, ten spectra were retaken after repolishing the

Ir crystal. The agreement between these two independent sets of data is excellent. The beams are indexed so that the longer side of the real-space unit cell is the y-direction in an (x,y) surface coordinate system.

3. Analysis

A convergent perturbative scheme known as the Layer-Doubling method (20), supplemented by a Reverse-Scattering-Perturbation formalism (20) when small interlayer spacings occurred, was used for the theoretical calculations. The scattering potential used for the Ir atoms is due to Arbman and Hörnfelt (21). It has been used successfully in our previous analyses (2, 3, 19, 22). Symmetry properties of the beams at normal incidence were exploited in the calculations. Six phase shifts were used (tests showed that this was sufficient within the error bars quoted here on structural parameters). The real part of the inner potential (V_0) was assumed to be 11eV, and this quantity was allowed to vary by a rigid shift of the energy scale for the comparison between theoretical and experimental I-V spectra. A homogeneous imaginary part of the muffin-tin constant of 5eV was used. The bulk Debye temperature used in the calculation was 280 K, and an enhancement factor of 1.4 was chosen for the surface mean-square vibrational amplitudes.

In the missing-row model shown in Figure 1, we varied the two topmost layer spacings and the lateral position of the second-layer atoms (while maintaining two mirror planes perpendicular to the surface). In addition, we also included in this model paired rows in the second layer and buckled rows in the third layer. These geometrical parameters are illustrated in Figure 2 and the values chosen for them are

shown in Table 1. The distances between the adjacent rows of atoms in the second layer in the [001] crystallographic direction are β and $2a-\beta$. The deviation from the normal distance in the second layer is $\Delta\beta = \beta - a$. The spacings between the atoms of the buckled rows in the third-layer and the first-layer atoms are δ_1 and δ_2 as shown in Figure 2. The spacing between the atoms of a buckled row is $\Delta\delta = \delta_1 - \delta_2$. The spacing between the different layers is defined here as the nearest distance between the nuclear planes in the successive layers. In the sawtooth model shown by position A in Figure 3, the geometrical position of the top-layer atom is varied in two different schemes as indicated by A_1 and A_2 in Table 1. In the A_1-sawtooth model, the top-layer atom is moved perpendicularly to the (110) surface while remaining directly over a third-layer atom. In the A_2-sawtooth model, the top-layer atom is moved perpendicularly to the (111) facet over a hollow site formed by two second-layer atoms and one third-layer atom. The hollow-on-facet model, as indicated by position B in Figure 3, is similar to the A_2-sawtooth model, but uses a different hollow site on the (111) facets: the top-layer atom moves perpendicularly to the (111) facet over a hollow site formed by one second-layer atom and two third-layer atoms. In the ridge model, as indicated by position C in Figure 3, the top-layer atom is located on a bridged site of the ridge of the missing-row model. A detailed list of the geometrical parameters varied in the different models is presented in Table 1.

4. Results

The agreement between experiment and theory is quantified by five R-factors and their average, which include the Zanazzi-Jona R-factor and

the Pendry R-factor. These are the R-factors ROS, R1, R2, RRZJ and RPE which were already applied in a number of LEED analyses (23).

The best five-R-factor average for each model is listed Table 2 (with interpolation between calculated geometries). The sawtooth model of Bonzel and Ferrer performs nearly as well as the simple (two-layer relaxed) missing-row model. The best five-R-factor averages for the sawtooth and the simple missing-row models are 0.31 and 0.28, respectively. The hollow-on-facet and ridge models are much worse. The missing-row model with paired rows in the second layer and buckled rows in the third layer (five-R-factor average of 0.25) is clearly the best model among all those we have considered. Plots of the five-R-factor average as a function of d_{12}, d_{23} and d_{34} are shown in Figure 4. Plots of $\Delta\beta$, $\Delta\delta$ and V_0 are displayed in Figures 5 - 7. The best values for d_{12}, d_{23}, d_{34}, $\Delta\beta$, $\Delta\delta$ and V_0 are determined by interpolation of these curves. This yields the best values for d_{12}, d_{23} and d_{34} of about 1.19 Å, 1.20 Å and 1.28 Å, which correspond to 12.3%, 11.6% and 6.0% contraction relative to the bulk interlayer spacing of 1.3585 Å. The rows of atoms in the second layer are shown to move towards each other by a small distance of about 0.07 Å; the displacements are towards the missing-row vacancies. Buckled rows (cf. Figure 2) are found in the third layer and the interlayer spacing distance between the buckled atoms is determined to be about 0.23 Å. The inner potential is found to be 10eV.

These results are in good agreement with those found in Au(110)-(1x2) by LEED (18) and Pt(110)-(1x2) by energy-minimization calculations (24). Table 3 shows a comparison of the best geometrical parameters

obtained for these surfaces. The results for these three surfaces are very similar except that the Au(110)-(1x2) surface has a larger first-layer contraction and a smaller second-layer contraction. Table 4 shows a comparison of the bond lengths between atoms in the top three layers for the Ir, Pt and the Au(110) surfaces. For both the Ir and Pt (110) surfaces, five out of seven bonds show a contraction, while on the Au(110) surface, only four show a contraction. But, on the whole, the results for Ir, Pt and Au are remarkably close. This is especially encouraging for a system in which many structural parameters are allowed to vary independently. We suggest that a LEED analysis of Pt(110)-(1x2) be done to confirm for that case also the missing-row model (with a three-layer relaxation).

Multi-layer relaxation now appears to occur frequently at relatively open metal surfaces (25), including fcc(110), bcc(100), bcc(211), bcc(310), bcc(210) and hcp(10$\bar{1}$0). Since multilayer relaxation has resolved several problematic structures, it may help resolve others. In particular, the W(100)-c(2x2) rearrangement (26) seems a good candidate for deeper-layer relaxations: The current best models involve unrealistically small bond lengths between the two topmost atomic layers, which could be accommodated by second- (and deeper-) layer relaxations that respect the observed prong symmetry.

Finally, a comment on the issue of the relatively easy (1x2) to (1x1) structural transition for these fcc(110) surfaces in the presence of certain adsorbates, which would appear to require excessively high metal diffusion rates (1). We believe that there is no contradiction, if one accepts the explanation proposed by Campuzano et al. (27) for

the analogous problem of the temperature-induced Au(110)-(1x2) to (1x1) phase transition. This would be an order-disorder transition requiring relatively little mass transport and causing a modest increase in diffuse intensity.

5. Conclusions

Based on the results of a LEED analysis, the missing-row model with paired rows in the second layer and buckled rows in the third layer is the best among all the models we have tested (the missing-row model, the missing-row model with row pairing in the second layer, the paired-row model, the buckled surface model, the Bonzel and Ferrer model, the hollow-on-facet model and the ridge model). The optimum values for d_{12}, d_{23}, d_{34}, $\Delta\beta$ and $\Delta\delta$ are 1.19 ± 0.07 Å, 1.20 ± 0.07 Å, 1.28 ± 0.07 Å, 0.1 ± 0.1 Å and 0.23 ± 0.07 Å, respectively. This result agrees well with a similar LEED result for Au(110)-(1x2) and an energy-minimization calculation for Pt(110)-(1x2).

Acknowledgements

We thank both Drs. W. Moritz and M. S. Daw for helpful discussions and for making their results available to us prior to publication. This work was supported in part by the Director, Office of Energy Research, Office of Basic Energy Sciences, Materials Sciences Division of the U.S. Department of Energy under contract No. DE-AC03-76SF00098.

REFERENCES

1. H. P. Bonzel and S. Ferrer, Surface Sci. 118, L263 (1982).

2. C.-M. Chan, M. A. Van Hove, W. H. Weinberg, and E. D. Williams, Solid State Commun. 30, 47 (1979).

3. C.-M. Chan, M. A. Van Hove, W. H. Weinberg, and E. D. Williams, Surface Sci. 91, 440 (1980).

4. D. L. Adams, H. B. Nielsen, M.A. Van Hove and A. Ignatiev, Surface Sci. 104, 47 (1981).

5. K. Müller, private communication.

6. W. Moritz and D. Wolf, Surface Sci. 88, L29 (1979); J. R. Noonan and H. L. Davis, J. Vac. Sci. Techol. 16, 587 (1979).

7. H. L. Davis, private communication.

8. J. D. Wrigley and G. Ehrlich, Phys. Rev. Letters 44, 661 (1980).

9. I. K. Robinson, Phys. Rev. Letters 50, 1145 (1983).

10. G. Binnig, H. Rohrer, Ch. Gerber, and E. Weibel, Surface Sci. 131, L379 (1983).

11. L. D. Marks, Phys. Rev. Letters 51, 1000 (1983).

12. S. H. Overbury, W. Heiland, D. M. Zehner, S. Datz and R. S. Thoe, Surface Sci. 109, 238 (1981); Y. Kuk, L. C. Feldman and I. K. Robinson, Surface Sci. 138, L168 (1984).

13. K. H. Rieder, T. Engel and N. Garcia, Proc. 4th ICSS - 3rd ECOSS, Suppl. "Le Vide Les Couches Minces" No. 201, p. 861 (1980).

14. M. Manninen, J. K. Nørskov and C. Umrigar, Surface Sci. 119, L393 (1982).

15. A. M. Lahee, W. Allison, R. F. Willis, K. H. Rieder, Surface Sci. 126, 654 (1983).

16. D. Tomanek, H. J. Brocksch and K. H. Bennemann, Surface Sci. 138, L129 (1984); H. J. Brocksch and K. H. Bennemann, contribution at First International Conference on the Structure of Surfaces, University of California, Berkeley, 1984.

17. T. Takai, T. Halicioglu and W. A. Tiller, contribution at First International Conference on the Structure of Surfaces, University of California, Berkeley, 1984.

REFERENCES (continued)

18. W. Moritz and D. Wolf, Surface Sci. to be published.

19. C.-M. Chan, K. L. Luke, M. A. Van Hove, W. H. Weinberg and S. P. Withrow, Surface Sci. 78, 386 (1978).

20. M. A. Van Hove and S. Y. Tong, Surface Crystallography by LEED, Springer, Berlin (1979).

21. G. O. Arbman and S. Hörnfelt, J. Phys. F2, 1033 (1972).

22. C.-M. Chan, S. L. Cunningham, M. A. Van Hove, W. H. Weinberg and S. P. Withrow, Surface Sci. 66, 394 (1977).

23. M. A. Van Hove and R. J. Koestner, in "Determination of Surface Structure by LEED," Eds. P. M. Marcus and F. Jona, Plenum Press (New York) 1984, p. 357. R. J. Koestner, M. A. Van Hove and G. A. Somorjai, Surface Sci. 107, 439 (1981).

24. M. S. Daw, private communication.

25. F. Jona, J. A. Strozier, Jr. and P. M. Marcus, in "The Structure of Surfaces," Proc. ICSOS-1, Eds. M. A. Van Hove and S. Y. Tong, Springer Series in Surface Sciences 2, Springer-Verlag (Heidelberg), 1985, p. 92.

26. R. A. Barker, P. J. Estrup, F. Jona and P. M. Marcus, Sol. St. Commun. 25, 375 (1978); J. A. Walker, M. K. Debe and D. A. King, Surface Sci. 104, 405 (1981).

27. T. C. Campuzano, A. M. Lahee and G. Jennings, Surface Sci. 152/153, 68 (1985).

Table 1: Summary of the Geometrical Parameters Used in Different Models

Model*	Range of Geometrical Variables, in Å	Increment in the Variables, in Å
Missing-row	d_{12} = 0.6585 to 1.9885	0.07
Missing-row with row pairing in the second layer	d_{12} = 0.8585 to 1.7585	0.1
	d_{23} = 0.8585 to 1.7585	0.1
	$\Delta\beta$ = -0.8 to 1.6	0.4
Missing-row with paired rows in the second layer and buckled rows in the third layer	d_{12} = 1.0785 to 1.4285	0.07
	d_{23} = 1.0785 to 1.4285	0.07
	d_{34} = 1.0785 to 1.4285	0.07
	$\Delta\beta$ = -0.1 to 0.2	0.1
	$\Delta\delta$ = -0.42 to 0.42	0.07
A_1 Sawtooth	d_{12} = 1.1485 to 1.4985	0.07
	d_{23} = 1.0788 to 1.6385	0.07
A_2 Sawtooth	ℓ = 2.3094 to 3.1925	0.07
	d_{23} = 1.0788 to 1.6385	0.07
B Hollow-on-Facet	ℓ = 2.3094 to 3.1925	0.07
C Ridge	d_{12} = 0.6585 to 1.9885	0.07

A_1 = The top-layer atom is sitting on top of a third-layer atom.

A_2 = The top-layer atom is sitting in a hollow site perpendicularly to the (111) facet formed by two second-layer atoms and one third-layer atom.

B = The top-layer atom is sitting in a hollow site perpendicularly to the (111) facet formed by one second-layer atom and two third-layer atoms.

C = The top-layer atom is sitting on the short-bridged site of the ridge.

d_{12} = The spacing between the first and second layers of atoms.

d_{23} = The spacing between the second and third layers of atoms.

d_{34} = The spacing between the third and fourth layers of atoms.

$\Delta\beta$ = The change in inter-row distance in the second layer of atoms, referred to the bulk.

$\Delta\delta$ = The interlayer spacing between the buckled atoms in the third layer.

ℓ = The bond length between atoms in the top layer and atoms in a nearby (111) facet.

*(See Figures 1, 2 and 3)

Table 2: A Summary of the R-Factor Analysis

Model	Geometrical Parameters, in Å	V_o, in eV	Averaged R-Factor
Missing-row	d_{12} = 1.2007	9	0.2829
Missing-row with row pairing only	d_{12} = 1.1772 d_{23} = 1.3585 $\Delta\beta$ = 0.0000	11	0.2872 (see Figure 2)
Missing-row with paired rows in the second layer and buckled rows in the third layer	d_{12} = 1.1908 d_{23} = 1.2011 d_{34} = 1.2804 $\Delta\beta$ = 0.0656 $\Delta\delta$ = 0.2294	10	0.2468
A_1 Sawtooth	d_{12} = 1.1780 d_{23} = 1.4236	10	0.3085
A_2 Sawtooth	d_{12} = 1.1776 y = 0.0000 z = 1.7932 d_{23} = 1.4285	10	0.3069
B Hollow-on-Facet	d_{12} = 1.1365 y = 0.0000 z = 2.7248	4	0.3569
C Ridge	d_{12} = 1.4160	6	0.3918

Table 3: A Comparison of the Best Geometrical Parameters for the (110)-(1x2) Surface Reconstructions of Ir, Pt and Au

	Ir(110)-(1x2)		Pt(110)-(1x2) (24)		Au(110)-(1x2) (18)	
	Å	α %*	Å	α %	Å	α %
d_{12}	1.19	-12.3	1.18	-14.4	1.15	-20.1
d_{23}	1.20	-11.6	1.26	-9.4	1.35	-6.3
d_{34}	1.28	-6.0	1.32	-5.0	1.35	-6.3
Δβ	0.07		0.10		0.14	
Δδ	0.23		0.12		0.24	

*α is the percent deviation from the bulk value.

Table 4: A Comparison of the Bond Lengths Between the Top-Three-Layer Atoms For the Ir, Pt and Au (110)-(1X2) Surfaces

	Ir(110)-(1X2)		Pt(110)-(1X2) (24)		Au(110)-(1X2) (18)	
	Å	α %*	Å	α %	Å	α %
r_{12}	2.66	-2.1	2.64	-5.0	2.80	-2.8
r_{14}	2.58	-3.5	2.56	-7.9	2.74	-5.0
r_{23}	2.62	-3.6	2.68	-3.7	2.79	-3.3
r_{24}	2.75	2.2	2.81	0.9	3.01	4.4
r_{25}	2.67	-0.2	2.70	-2.9	2.94	2.0
r_{35}	2.77	2.9	2.83	1.8	2.96	2.7
r_{45}	2.68	-1.4	2.71	-2.4	2.84	-1.5

*α is the percent deviation from the bulk value.

FIGURE CAPTIONS

Figure 1 (a), (b) Top and side views of a hard-sphere representation of the missing-row model.

Figure 2 The geometrical parameters used in the missing-row model with paired rows in the second layer and buckled rows in the third layer, where a = 3.84Å is the bulk-like spacing between rows in the [001] crystallographic direction. Displacements from the ideal bulk-like positions are exaggerated for clarity.

Figure 3 (a) Top view of a hard-sphere representation of several alternate models. Site A is the sawtooth model; Site B is the hollow-on-facet model; and Site C is the ridge model.

(b) Corresponding side view of (a).

Figure 4 Plots of the five-R-factor average as a function of d_{12}, d_{23} and d_{34} for the missing-row model with three-layer relaxation.

Figure 5 Plot of the five-R-factor average as a function of $\Delta\beta$ for the missing-row model with three-layer relaxation.

Figure 6 Plot of the five-R-factor average as a function of $\Delta\delta$ for the missing-row model with three-layer relaxation.

Figure 7 Plot of the five-R-factor average as a function of V_0 for the missing-row model with three-layer relaxation.

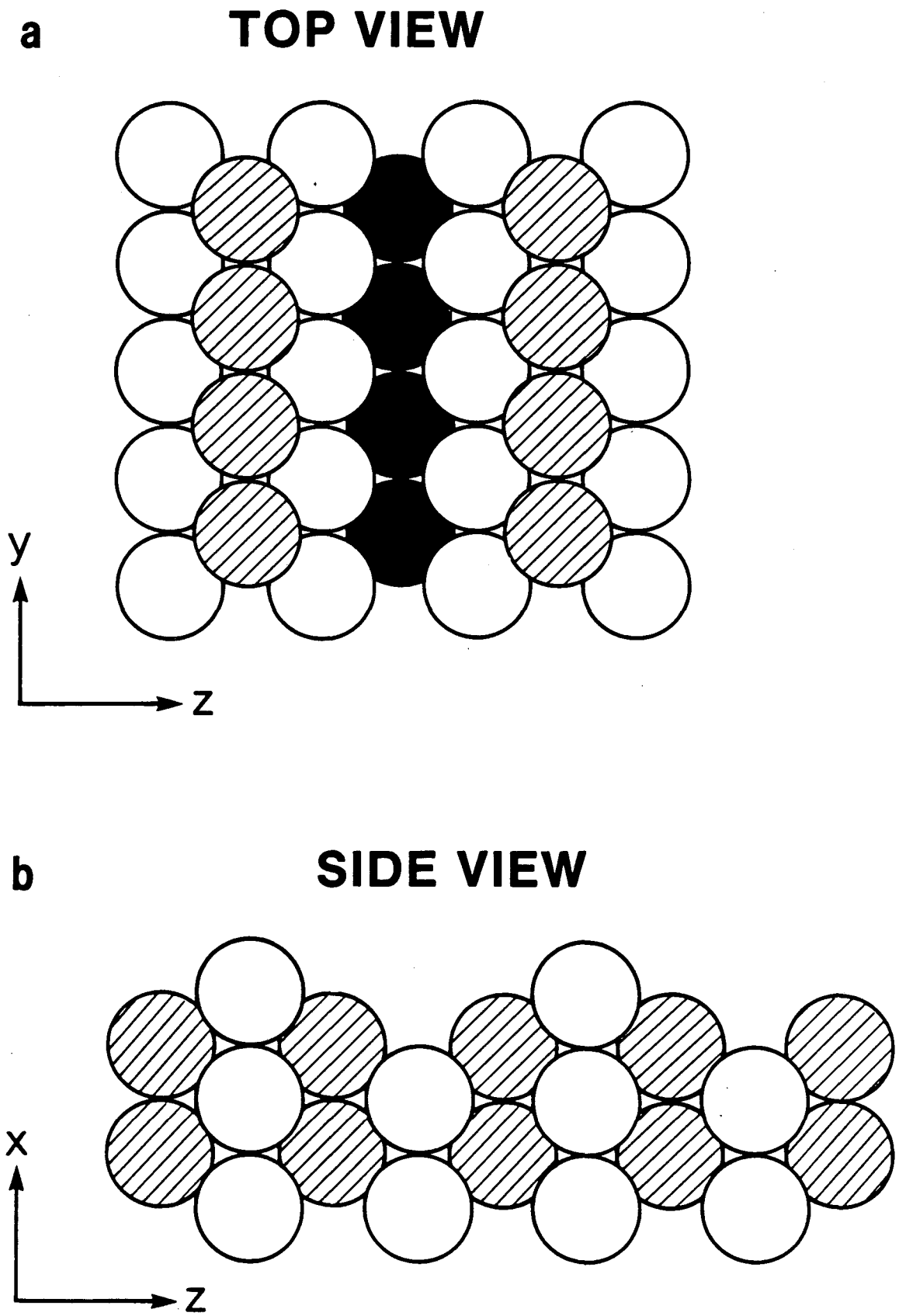

Fig. 1.

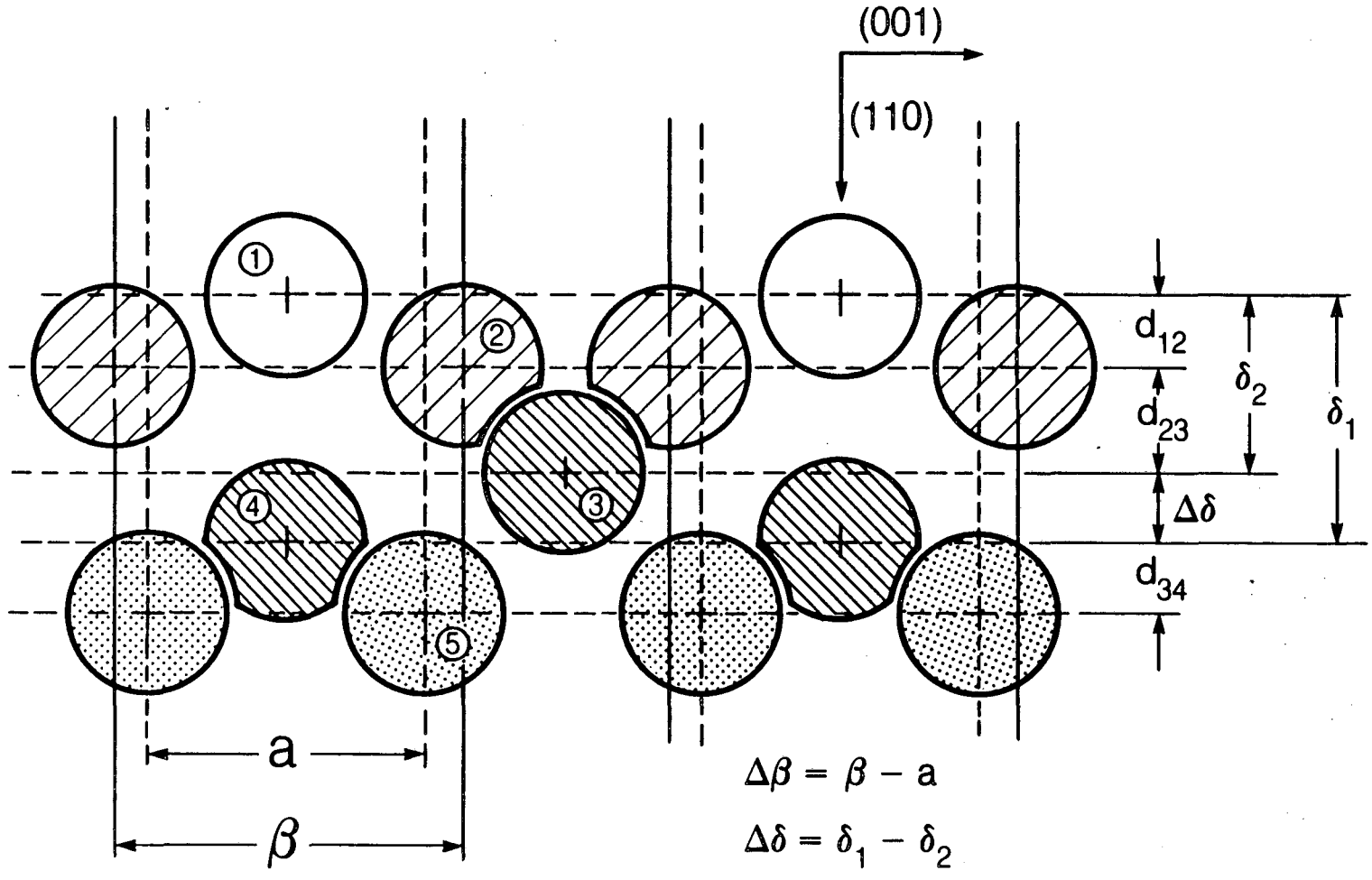
fcc (110) – (1 × 2) missing-row model
(001)
(110)
①
②
③
④
⑤
d_{12}
d_{23}
$\Delta\delta$
d_{34}
δ_2
δ_1
a
β
$\Delta\beta = \beta - a$
$\Delta\delta = \delta_1 - \delta_2$
XBL 857-11651

Fig. 2

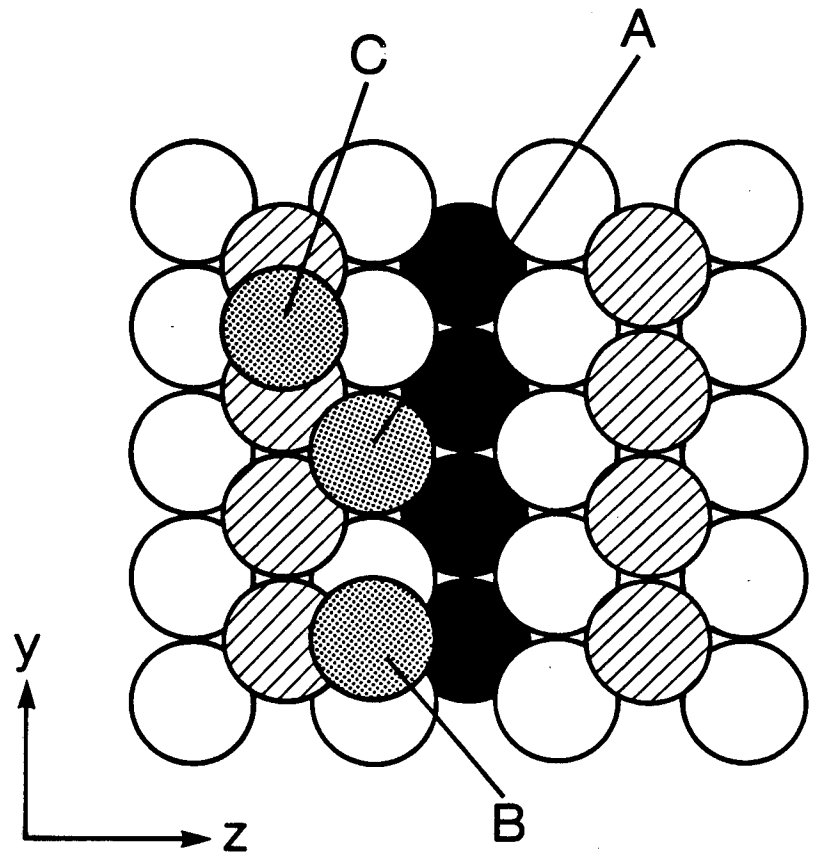

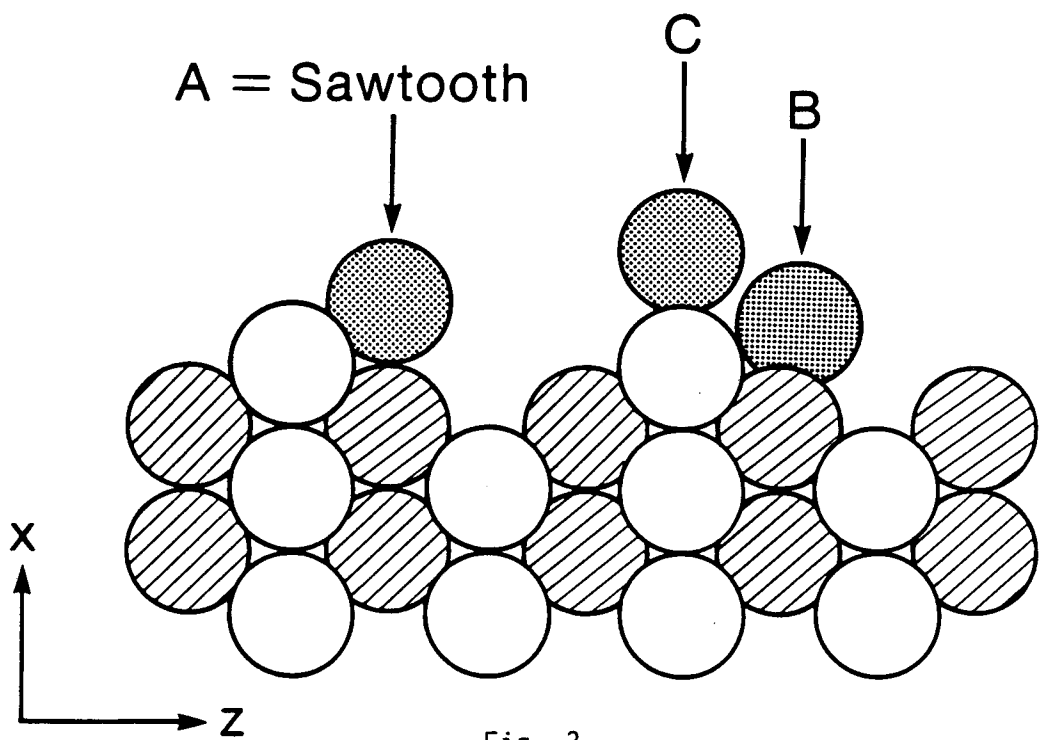

Fig. 3.

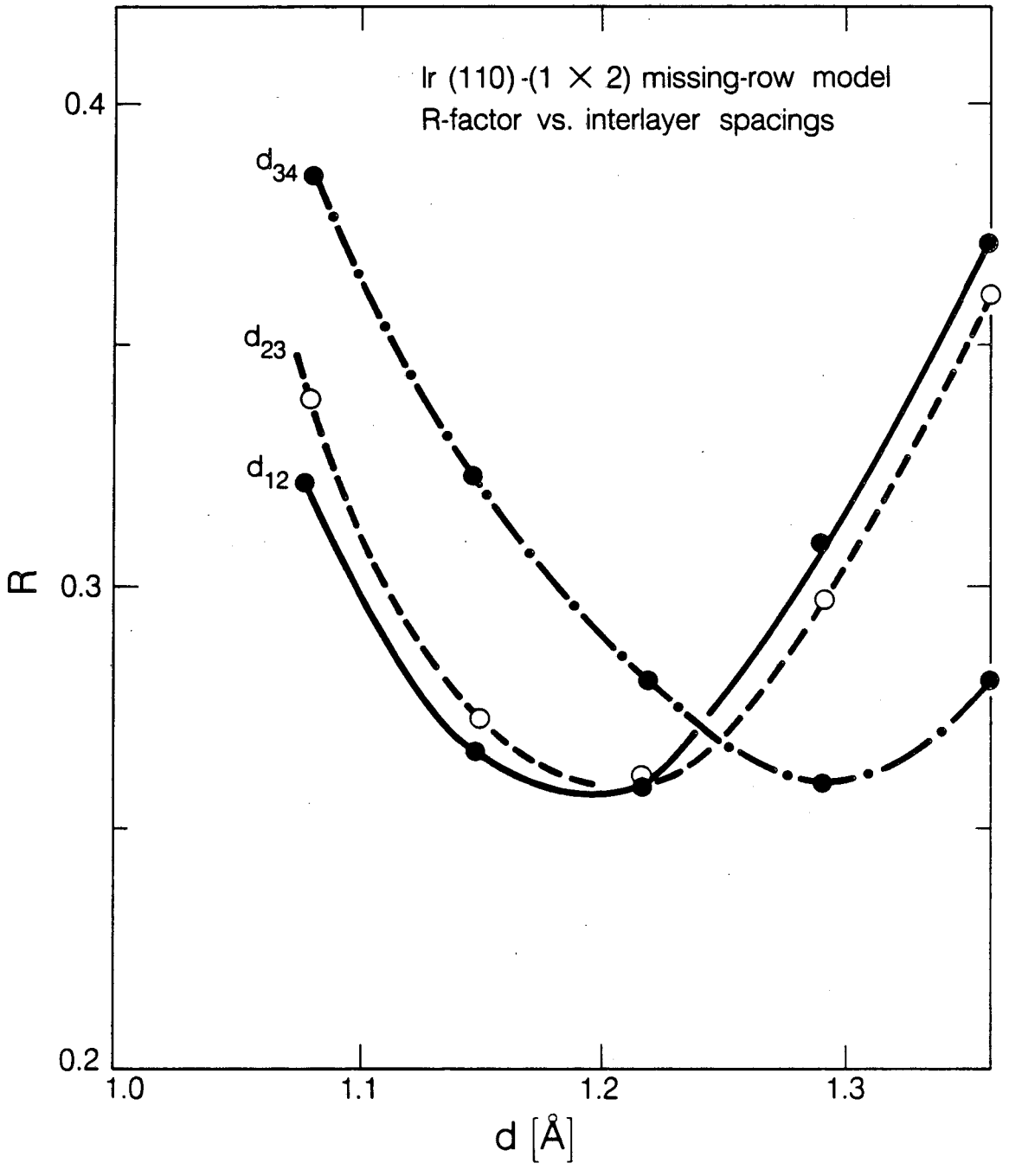

XBL 857-11647

Fig. 4.

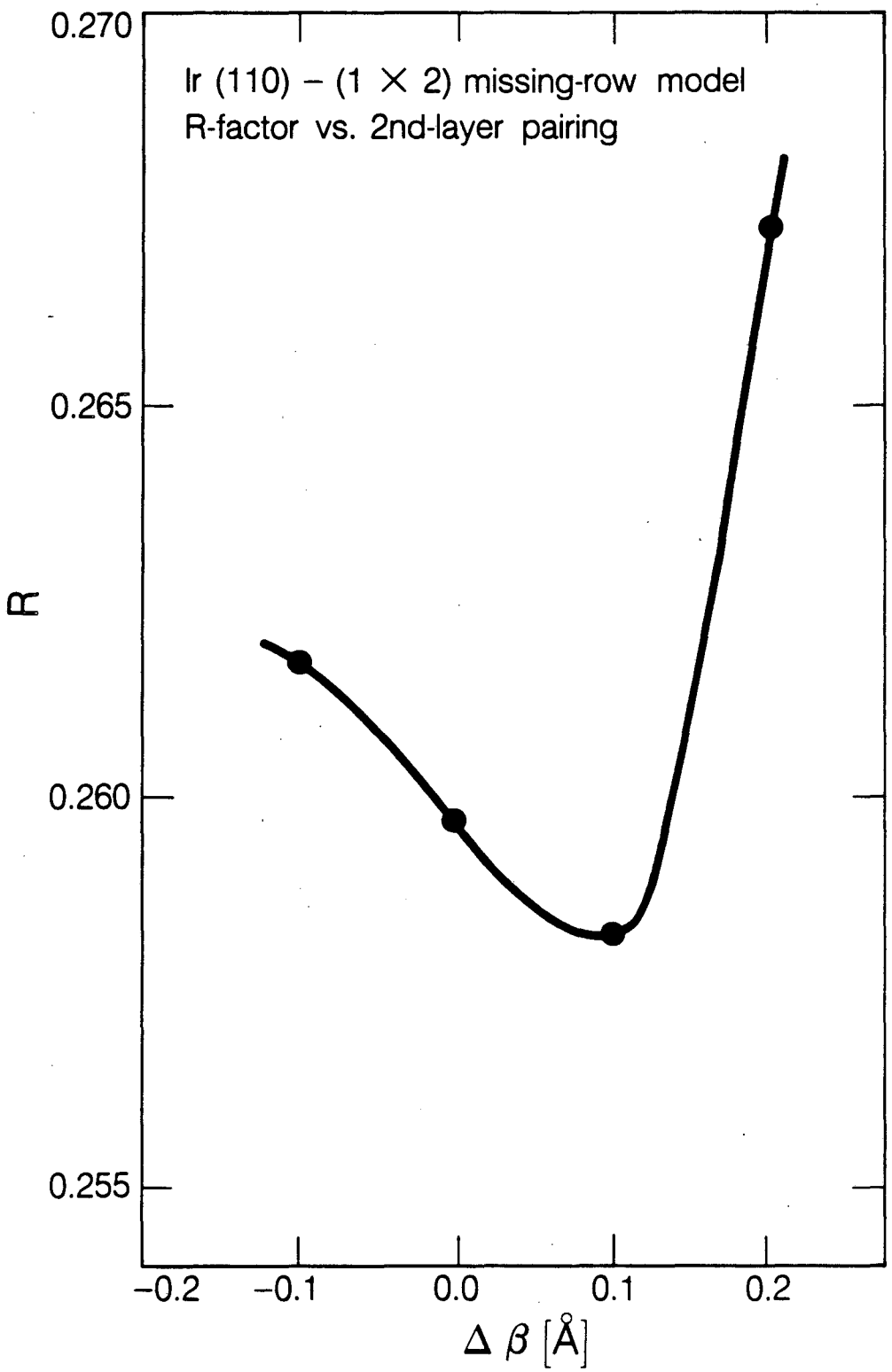
Ir (110) – (1 × 2) missing-row model
R-factor vs. 2nd-layer pairing
0.270
0.265
0.260
0.255
R
−0.2
−0.1
0.0
0.1
0.2
Δ β [Å]
XBL 857-11649

Fig. 5.

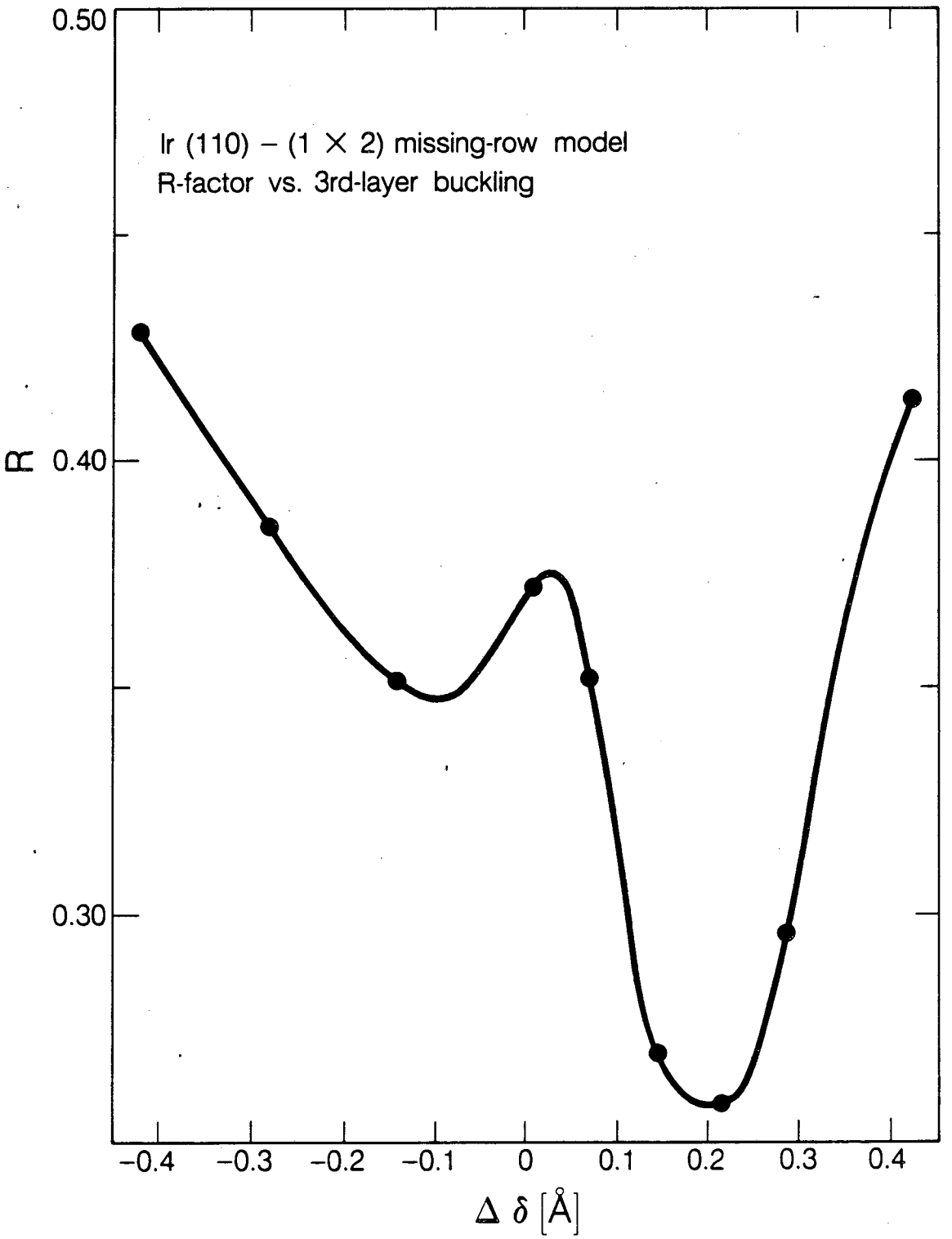
Ir (110) – (1 × 2) missing-row model
R-factor vs. 3rd-layer buckling
0.50
0.40
0.30
R
−0.4
−0.3
−0.2
−0.1
0
0.1
0.2
0.3
0.4
Δ δ [Å]
XBL 857-11648

Fig. 6.

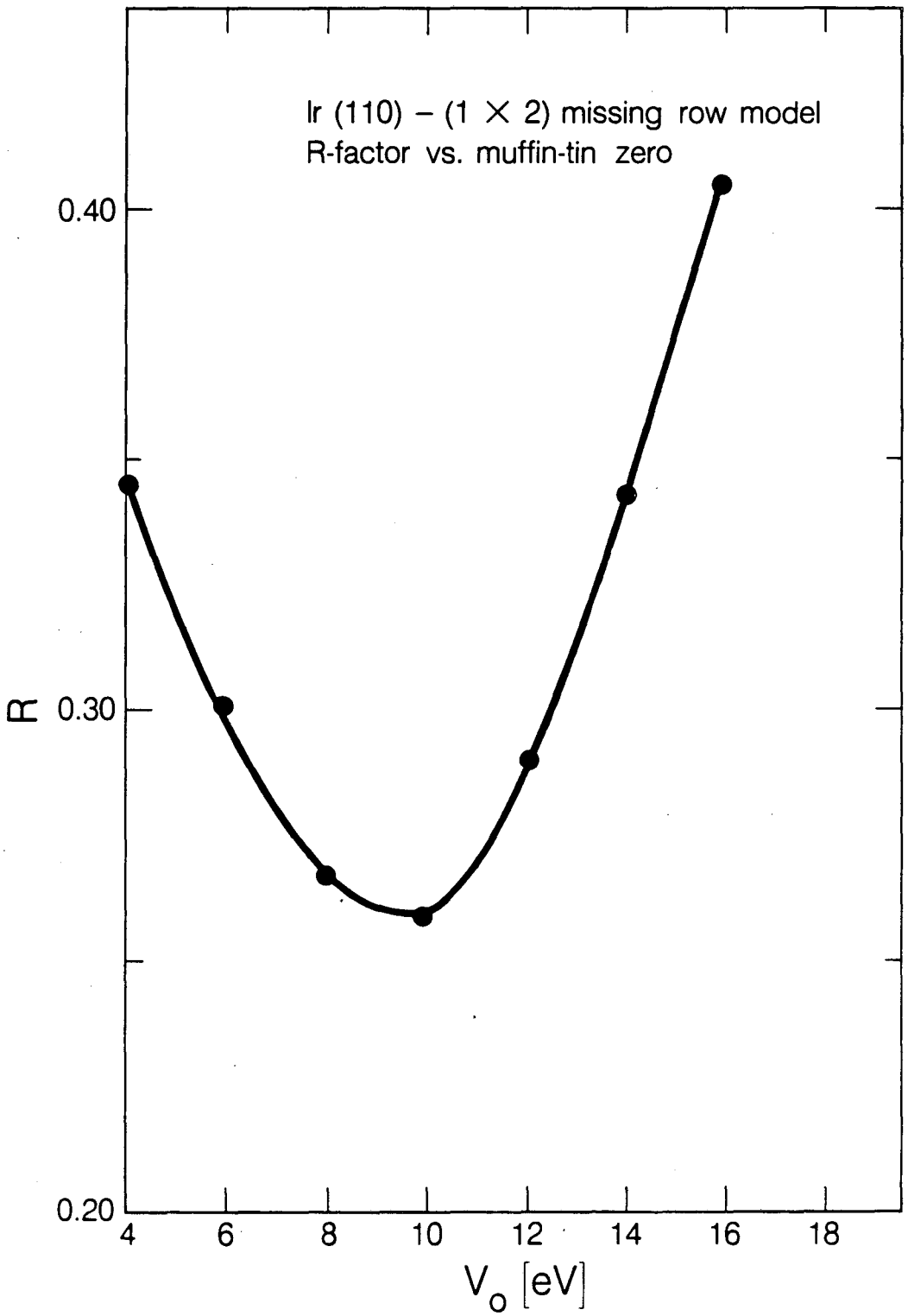
Ir (110) – (1 × 2) missing row model
R-factor vs. muffin-tin zero
0.40
R 0.30
0.20
4
6
8
10
12
14
16
18
V_o [eV]
XBL 857-11650

Fig. 7.

LAWRENCE BERKELEY LABORATORY
TECHNICAL INFORMATION DEPARTMENT
UNIVERSITY OF CALIFORNIA
BERKELEY, CALIFORNIA 94720